



Preparation and characterization of dispersive carbon-coupling ZnO photocatalysts

Hsuan-Fu Yu ^{a,b,*}, Hung-Yu Chou ^a

^a Department of Chemical and Materials Engineering, Ceramic Materials Laboratory, Tamkang University, Taipei 25137, Taiwan

^b Energy and Opto-Electronic Materials Research Center, Tamkang University, Taipei 25137, Taiwan

ARTICLE INFO

Article history:

Received 21 May 2012

Received in revised form 23 August 2012

Accepted 5 September 2012

Available online 12 September 2012

Keywords:

Zinc oxide

Precipitation

Combustion

Coupled photocatalysts

Photocatalysis

ABSTRACT

Dispersive carbon-coupling ZnO particles (C/ZnO) with smaller particle sizes and higher specific surface area were produced using a method combining precipitation and combustion techniques. Glucose was added in the production procedure to act as fuel to conduct combustion reaction and as source to form tiny carbon particles in the C/ZnO. Physical and chemical properties of the prepared C/ZnO particles were investigated and photocatalytic abilities of these particles to photocatalytically decompose the methylene blue in water under 365-nm UV light irradiation were kinetically studied. The prepared C/ZnO particles exhibited higher photocatalytic ability than the ZnO particles and the P25. The C/ZnO particles calcined at 900 °C possessed the best photocatalytic performance and had a reaction rate constant (k_m) of $0.859 \text{ L} \cdot (\text{g} \cdot \text{min})^{-1}$, which exhibited much higher photocatalytic ability than the ZnO calcined at 700 °C ($k_m = 0.326 \text{ L} \cdot (\text{g} \cdot \text{min})^{-1}$) and the P25 ($k_m = 0.371 \text{ L} \cdot (\text{g} \cdot \text{min})^{-1}$).

© 2012 Elsevier B.V. All rights reserved.

1. Introduction

ZnO with a hexagonal wurtzite structure is an n-type semiconductor material, which has wide-bandgap energy of 3.37 eV and exciton binding energy of 60 meV. ZnO, aside from TiO_2 , has been considered as a promising material for purification and disinfection of water and air, and remediation of hazardous waste, owing to its high activity, environment-friendly feature and lower cost [1–6]. Several methods have been used to prepare ZnO particles, such as precipitation [7–10], hydrothermal method [11–15], and spray pyrolysis [16–19]. In the application of ZnO photocatalyst, one major problem faced is the fast recombination rate of the photoinduced electrons and electron holes [20,21], which leads to a reduction of photocatalytic activity of the ZnO. Some efforts have been made to improve the photocatalytic activity of ZnO by coupling ZnO with metal or metallic oxide, like Ag [22–24], SnO_2 [25,26], Cu_2O [27] and TiO_2 [28]. ZnO photocatalysts coupled with metal or oxide may retard their electron–hole recombination rates by trapping the photoinduced electrons in the coupling phase and consequently could promote the photocatalytic abilities.

In this study, we proposed a simple method combining precipitation and combustion techniques to prepare carbon-coupling ZnO nanoparticles (C/ZnO). Glucose was used as fuel to carry out the required combustion reaction and as source to form tiny carbon particles to produce dispersive C/ZnO nanoparticles with high photocatalytic reactivity. The characteristics and photocatalytic activities of the C/ZnO

particles were investigated and were compared to those of the ZnO particles without carbons coupling (ZnO) and the P25 (a commercial TiO_2 photocatalyst product; Degussa, Germany).

2. Experimental detail

2.1. Sample preparation

Zinc nitrate hexahydrate ($\text{Zn}(\text{NO}_3)_2 \cdot 6\text{H}_2\text{O}$, 99% purity, Showa) was dissolved in distilled water to form an aqueous solution of 0.2 M. NH_4OH (28 wt.%, Tedia) was then added dropwise to the stirred aqueous solution until pH = 8. After being continuously stirred for 1 h, the solid precipitates were collected by centrifugal filtration and were dried in an oven at 90 °C. The mixture containing the dried precipitates, distilled water and glucose ($\text{C}_6\text{H}_{12}\text{O}_6$, 98% purity, Showa), in weight ratios of precipitates: distilled water: glucose = 1: 1.7: x (where x = 0 or 0.85), was ball-milled for 12 h, followed by drying at 90 °C. The added glucose acted as fuel to carry out combustion reaction at the follow-up thermal treatment. The dried ZnO precursor (i.e., x = 0) and the C/ZnO precursor (i.e., x = 0.85) were then heated up, in a muffle furnace, to different temperatures and isothermally treated at the designed temperature for 3 h.

2.2. Characterization

Thermal behavior of the ball-milled particles was investigated using a thermal analyzer STA 499F3 (Netzsch, Germany), which is capable of performing thermogravimetric analysis (TG) and differential scanning calorimetry (DSC) simultaneously for the same sample. The crystalline phases and crystal structure existing in the specimen were

* Corresponding author at: Department of Chemical and Materials Engineering, Ceramic Materials Laboratory, Tamkang University, Taipei 25137, Taiwan. Tel.: +886 2 26209887; fax: +886 2 26209887.

E-mail address: hfyu@mail.tku.edu.tw (H.-F. Yu).

examined by X-ray diffraction analysis (XRD; X-ray wavelength 0.154056 nm; D8A; Bruker, Germany). Average crystallite sizes of the obtained ZnO particles were estimated by employing Scherrer's equation in the corresponding profiles of the (101) XRD peak for ZnO. Morphologies and sizes of the particles and the crystallites were observed using scanning electron microscopy (SEM; LEO 1530, Carl Zeiss, USA) and transmission electron microscopy (TEM; H-7100; Hitachi, Japan). Specific surface areas of the calcined specimens were measured using an automated BET sorptometer (Porous Materials, USA), operated at a liquid-nitrogen temperature of around $-196\text{ }^{\circ}\text{C}$. To examine the effect of the coupling carbons on the electron-hole recombination rate of the photo-excited ZnO, photoluminescence (PL) spectra of the specimens were measured using a fluorescence spectrophotometer (Hitachi F-2500, Japan), which used Xe lamp as excitation source at room temperature.

2.3. Photocatalytic activity determination

Photocatalytic activities of the ZnO and the C/ZnO particles were estimated by examining their abilities to photocatalytically decompose the MB in water. In a dark chamber, the tested particles of 0.01 g were dispersed in the aqueous solution of MB (10 μM , 200 mL) and the suspension so obtained was vigorously stirred for 10 min to attain the adsorption-desorption equivalence of MB on catalyst, which was confirmed by observing the change of concentration of the $\text{MB}_{(\text{aq})}$ using ultraviolet-visible spectroscopic analysis (UV-vis; Unicam UV500; Thermospectronic, UK). Then, the tested particles were irradiated using 365-nm ultraviolet (UV) lamps (8 W \times 2, Great Tide Instrument, Taiwan). The reaction system was maintained at about 25 $^{\circ}\text{C}$. After every 5 or 10 min UV exposure, 3 mL of the testing MB solution was sampled and was subjected to UV-vis analysis. The absorbance of the MB characteristic band at 664 nm in the obtained UV-vis spectrum was used to determine the concentration of MB in the solution. The concentration changes of $\text{MB}_{(\text{aq})}$ with time under the conditions described above were recorded and examined to determine the photocatalytic activities of the prepared nanoparticles. The specific reaction rate of photocatalyst used (k_m) for photocatalytic degradation of MB under 365-nm UV light was estimated [29] and was used as an index of photocatalytic activity of the prepared photocatalyst.

3. Results and discussion

3.1. Thermal behavior

Fig. 1(a) shows the TG & DSC curves of the ZnO precursor. The ZnO precursor on the course of heating experienced five major endothermic changes and resulted in totally about 34.5% loss in weight. The TG curve of the ZnO precursor was leveled off at the temperature above 300 $^{\circ}\text{C}$. The first endothermic change (the DSC peak with a peak temperature of 42 $^{\circ}\text{C}$) was due to evaporation of the physical adsorbed water. To examine the composition changes caused by the other four endothermic changes, the ZnO precursor was heated up to the pre-designed temperatures, without thermal soaking, and the resultant particles were XRD-examined. Fig. 1(b) gives the XRD patterns of the ZnO precursor dried or heated at 90 $^{\circ}\text{C}$, 170 $^{\circ}\text{C}$ and 300 $^{\circ}\text{C}$. The major crystalline phases detected in the specimens were $\text{Zn}_5(\text{NO}_3)_2(\text{OH})_8\cdot\text{H}_2\text{O}$ (ICDD # 24-1460) and $\text{Zn}_3(\text{OH})_4(\text{NO}_3)_2$ (ICDD # 52-0627) at 90 $^{\circ}\text{C}$, $\text{Zn}_3(\text{OH})_4(\text{NO}_3)_2$ at 170 $^{\circ}\text{C}$ and ZnO (ICDD # 65-3411) at 300 $^{\circ}\text{C}$. Based on the results shown in Fig. 1, the major reactions that occurred during the heating of the ZnO precursor are proposed as follows:

at 90–152 $^{\circ}\text{C}$ (corresponding to the DSC peaks at 107 $^{\circ}\text{C}$ and 127 $^{\circ}\text{C}$ in Fig. 1(a))

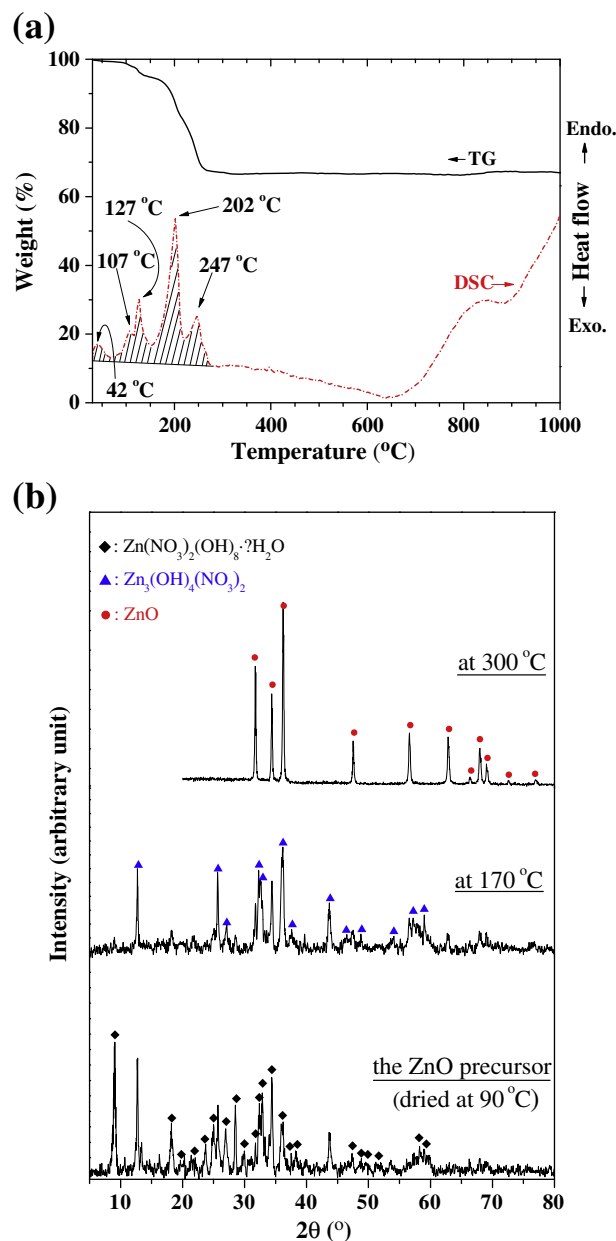
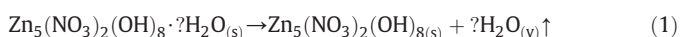
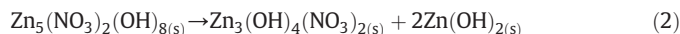


Fig. 1. (a) TG and DSC curves, operating at 4 $^{\circ}\text{C}/\text{min}$ heating rate and 30 mL/min air flow, of the ZnO precursor and (b) XRD patterns of the ZnO precursor dried or heated at different temperatures.



at 152–222 $^{\circ}\text{C}$ (corresponding to the DSC peak at 202 $^{\circ}\text{C}$ in Fig. 1(a))



at 222–300 $^{\circ}\text{C}$ (corresponding to the DSC peak at 247 $^{\circ}\text{C}$ in Fig. 1(a))



Heating the ZnO precursor at temperatures above 300 $^{\circ}\text{C}$ produces pure crystalline ZnO with a hexagonal wurtzite structure.

Fig. 2(a) gives the TG & DSC curves of the C/ZnO precursor. During heating, the C/ZnO precursor undertook four endothermic changes and one strong exothermic change, which caused totally about 61.5% loss in weight. XRD analysis (see Fig. 2(b)) indicated that the major crystalline

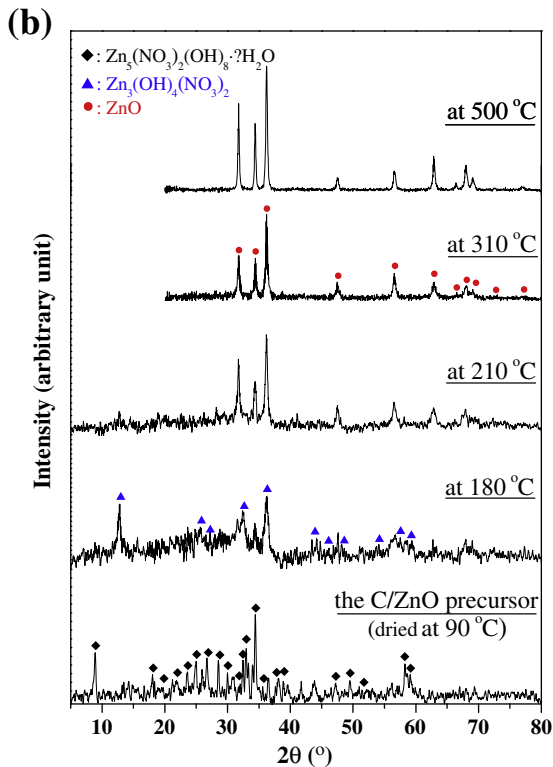
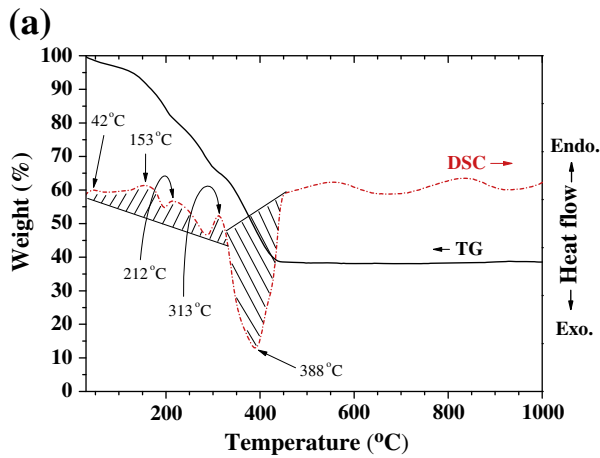


Fig. 2. (a) TG and DSC curves, operating at 4 °C/min heating rate and 30 mL/min air flow, of the C/ZnO precursor and (b) XRD patterns of the C/ZnO precursor dried or heated at different temperatures.

phases existing in the dried or heated C/ZnO precursor were $\text{Zn}_3(\text{NO}_3)_2(\text{OH})_8 \cdot ?\text{H}_2\text{O}$ at 90 °C and $\text{Zn}_3(\text{OH})_4(\text{NO}_3)_2$ at 180 °C; above 210 °C, the C/ZnO precursor started to transform to crystalline ZnO. Fig. 3 shows the TG & DSC curves of glucose. It indicated that glucose started to melt at 143 °C (the DSC peak with the peak temperature at 163 °C) and began to caramelize and/or decompose at about 178 °C (the DSC peak with a peak temperature of 203 °C), which accompanied with about 12% loss in weight. Above 270 °C, two successive strong oxidation reactions (combustions) were taken place in the glucose specimen. The first oxidation reaction (the DSC peak with a peak temperature of 342 °C in Fig. 3) should be due to the carbonization of the specimen and the second one (the DSC peak with a peak temperature of 483 °C in Fig. 3) should be ascribed to the oxidation of residual carbons to form carbon dioxide. After the second oxidation reaction, all of the residual carbons were burned out and the TG curve was reached to zero weight.

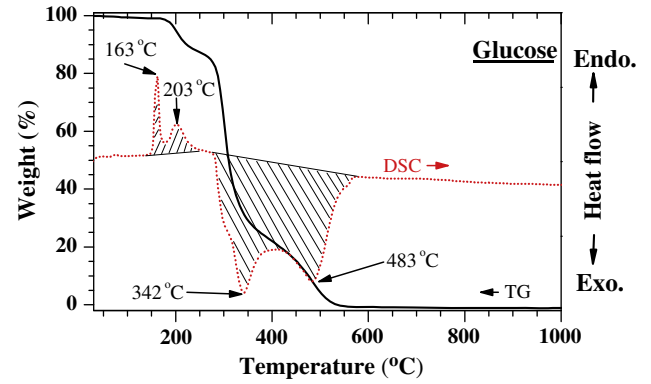


Fig. 3. TG and DSC curves, operating at 4 °C/min heating rate and 30 mL/min air flow, of glucose.

Effects of glucose addition on the thermal behavior of the C/ZnO precursor were investigated by comparing the TG & DSC curves and the XRD patterns of the C/ZnO precursor (Fig. 2) with those of the ZnO precursor (Fig. 1) and glucose (Fig. 3). Adding glucose to the solid precipitates can prevent the formation of $\text{Zn}_3(\text{OH})_4(\text{NO}_3)_2$ during ball-milling step. During heating, the major reaction steps of the C/ZnO precursor below 325 °C were similar to those of the ZnO precursor (i.e., Eq. (1)–Eq. (4)); however, the temperature range of each change became broader, which was due to the existence of glucose melt and its derivatives. Above 325 °C, the combustion (a strong exothermic reaction) occurred in the C/ZnO precursor (the DSC peak with a peak temperature of 388 °C in Fig. 2(a)) was ascribed to the glucose addition. Unlike the thermal behavior of glucose (see the DSC curve in Fig. 3), only one exothermic peak was detected in the DSC curve of the C/ZnO precursor. It was suspected that the added glucose in the C/ZnO precursor underwent only carbonization at temperature range from 325 °C to 460 °C and formed stable carbons in the specimen. To verify the existence of carbons in the C/ZnO calcined at temperatures above 460 °C, the calcined C/ZnO particles were examined by TEM with elemental mapping. Fig. 4, for instance, shows the TEM image and its elemental mappings of Zn, O and C of the C/ZnO at 900 °C. The ZnO crystallites (the dark and big ones in the TEM image) are surrounded by loose carbon tiny particles (the light gray particles in the TEM image). Accordingly, the carbon particles survived the calcination of C/ZnO, even at 900 °C, and some of these tiny carbon particles were coupled to the ZnO crystallites. The addition of glucose in the production procedure can produce carbon-coupling ZnO particles.

3.2. Powder characteristics

XRD analysis indicated that the ZnO and the C/ZnO particles calcined at temperatures ranging from 500 °C to 1000 °C were all composed of crystalline ZnO monophase with a hexagonal wurtzite structure. Fig. 5 gives the average sizes of the crystallites in the ZnO and the C/ZnO calcined at different temperatures. Increasing calcination temperature promoted the growth of ZnO crystallites, but the addition of glucose in the production procedure produced smaller ZnO crystallites. Fig. 6 is SEM images of the calcined ZnO and the calcined C/ZnO. The particle sizes of the ZnO and the C/ZnO increased with raising calcination temperature. At the same calcination temperature, the C/ZnO particles were smaller and more dispersive than the ZnO particles. In the C/ZnO precursor, the added glucose was uniformly distributed on the surfaces of the Zn^{2+} -containing precipitates through ball-milling. Heating the C/ZnO precursor at temperature above 325 °C triggered the combustion of glucose derivatives and produced a large amount of gasses between the solid particles. The combustion gasses expanded the distances between the particles and reduced the degree of particle agglomeration, resulting in more dispersive particles. Fig. 7 shows the specific

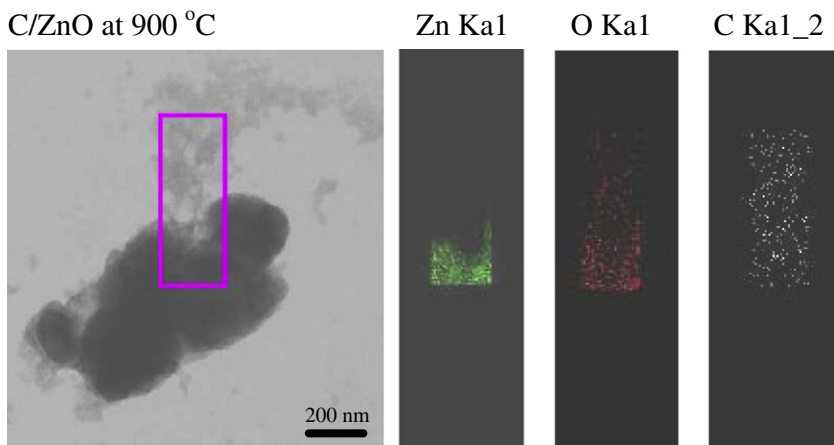


Fig. 4. TEM image and its elemental mapping of the C/ZnO calcined at 900 °C.

surface areas of the calcined ZnO and C/ZnO particles. The specific surface area of the ZnO and the C/ZnO specimens decreased with increasing calcination temperature and at the same calcination temperature, the C/ZnO particles had higher specific surface area than the ZnO particles. The results from the specific surface area measurement of particles are in good agreement with those observed from their SEM images.

3.3. Photocatalytic abilities

Fig. 8 shows the percentages of the $MB_{(aq)}$ in water photocatalytically decomposed by the calcined ZnO and the calcined C/ZnO particles, as well as the P25, after exposing to 365-nm UV light for 30 min. The P25 photocatalytically decomposed 45 mol% of the MB after 30 min. For the calcined ZnO particles, the photocatalytic ability increased with raising calcination temperature until 700 °C but greatly decreased when the calcination temperature was at or above 800 °C. Regardless of the calcination temperature used, the calcined ZnO particles all had less photocatalytic abilities than the P25. On the other hand, the calcined C/ZnO particles possessed very good photocatalytic abilities to decompose the MB in water. While the C/ZnO at 500 °C decomposed about 45 mol% of the MB, which was similar to that of the P25, the photocatalytic ability of the calcined C/ZnO particles increased with increasing calcination temperature. The C/ZnO particles calcined at 900 °C exhibited the best performance, which decomposed 73 mol% of the MB after exposing to 365-nm UV light for 30 min. The C/ZnO particles calcined at 1000 °C, which possessed larger particle sizes and smaller specific surface area, had its photocatalytic ability slightly lower than those of the C/ZnO particles

calcined at 800 and 900 °C. The C/ZnO particles calcined at temperatures ranging from 600 °C to 1000 °C all have much higher photocatalytic performance than the P25.

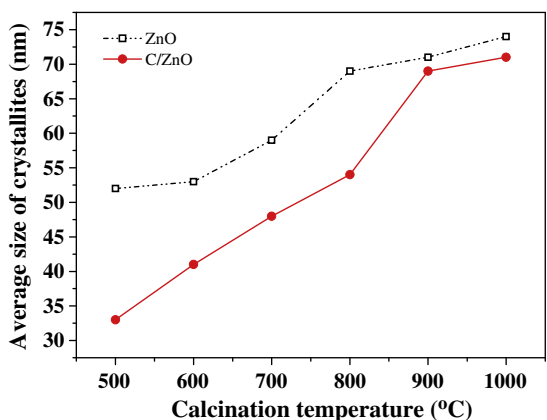


Fig. 5. Changes of average size of the ZnO crystallites, in the specimens of the ZnO and C/ZnO, with calcination temperature.

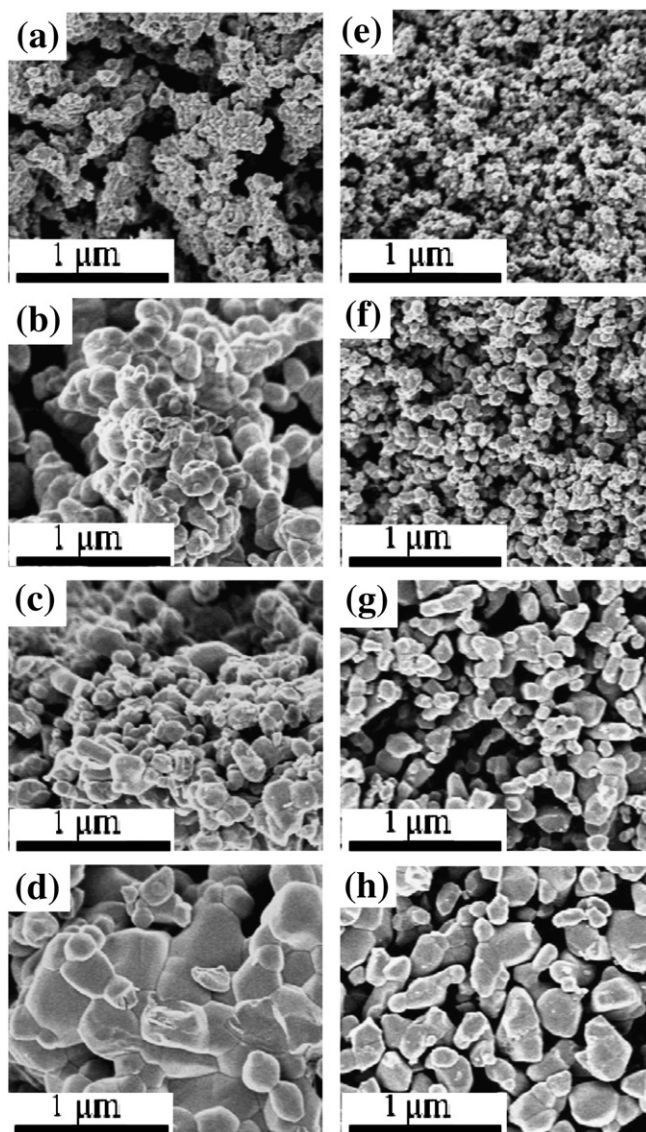


Fig. 6. SEM images of the ZnO calcined at (a) 500 °C, (b) 700 °C, (c) 900 °C, (d) 1000 °C, and the C/ZnO calcined at (e) 500 °C, (f) 700 °C, (g) 900 °C, and (h) 1000 °C.

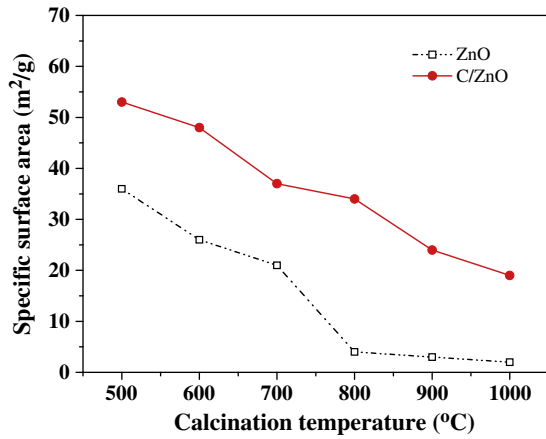


Fig. 7. Specific surface areas of the calcined ZnO and C/ZnO particles.

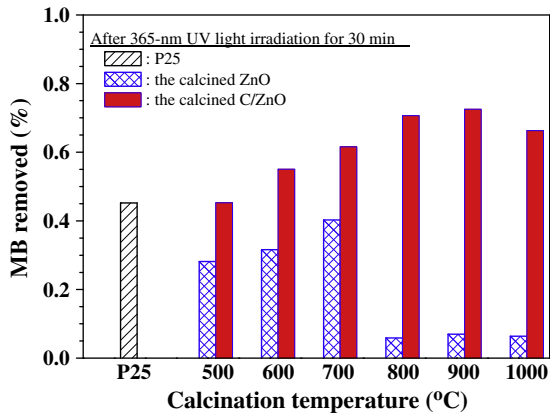


Fig. 8. Percentages of methylene blue photocatalytically decomposed by the calcined ZnO, the calcined C/ZnO and a commercial product P25 after exposing to 365-nm UV light for 30 min.

The photocatalytic abilities of the calcined ZnO and C/ZnO particles to decompose the $MB_{(aq)}$ were kinetically studied. During photocatalysis, the concentration changes of $MB_{(aq)}$ with reaction time were recorded and analyzed. It was found that the concentration of MB in water (C_{MB}), in all the cases, was exponentially decreased with reaction time (t). Fig. 9, for instance, shows the changes of C_{MB} with t during the course of MB photodecomposition catalyzed by the ZnO and the C/ZnO at 500 and 1000 °C, as well as the P25.

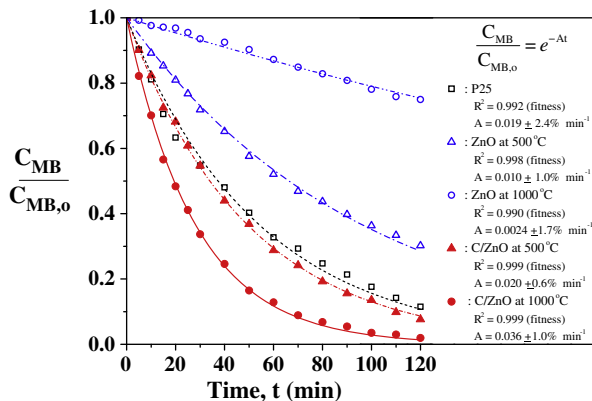


Fig. 9. Concentration changes of the $MB_{(aq)}$ during the course of photodecomposition catalyzed by the calcined ZnO and C/ZnO particles, as well as P25.

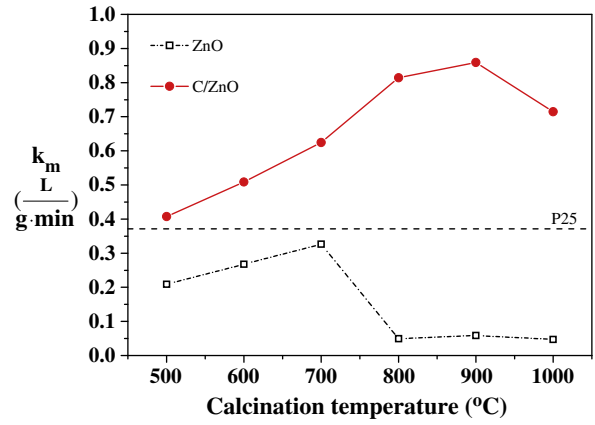


Fig. 10. Changes of the specific reaction rate (k_m) with calcinations temperature for the ZnO and the C/ZnO.

Fig. 10 shows the changes of k_m with calcination temperature for the calcined ZnO and C/ZnO, as well as the P25. k_m for the C/ZnO increased with calcination temperature until 900 °C, but further increasing the calcination temperature to 1000 °C caused a decrease in the corresponding k_m . The best performance of the calcined C/ZnO photocatalyst was that of the C/ZnO calcined at 900 °C ($k_m = 0.859 \text{ L} \cdot (\text{g} \cdot \text{min})^{-1}$). For the calcined ZnO, the changes of k_m with calcination temperature were similar to those of the calcined C/ZnO but the maximum value of k_m occurred at 700 °C, which had $k_m = 0.326 \text{ L} \cdot (\text{g} \cdot \text{min})^{-1}$. It is known that the reactivity of the semiconductor photocatalyst is greatly affected by its specific surface area and crystallinity. The particle with high degree of crystallinity is composed of large crystallites. The photocatalyst with high specific surface area or composed of large crystallites will exhibit better photocatalytic activity [29]. Raising the calcination temperature will increase the size of ZnO crystallites (see Fig. 5) but will decrease the specific surface area of the particles (see Fig. 7). Fig. 10 indicates that the optimum conditions to prepare the ZnO and the C/ZnO with the highest photocatalytic performance are to calcine the ZnO precursor at 700 °C and the C/ZnO precursor at 900 °C. Regardless of the calcination temperature used, all the calcined C/ZnO particles possess much better photocatalytic activity than the calcined ZnO and the P25.

As mentioned before, loose carbon tiny particles were surrounded and attached to the ZnO crystallites in the calcined C/ZnO specimens. To recognize the effect of these tiny carbon particles, other than the effects of the specific surface area and crystallite size of ZnO particles, on the photocatalytic activity of ZnO, the k_m values of the ZnO calcined at 500 °C (average ZnO crystallite size = 52 nm, specific surface area = 36 m^2/g) and the C/ZnO calcined at 800 °C (average ZnO crystallite size = 54 nm, specific surface area = 34 m^2/g) were compared. Although these two specimens were all composed of wurtzite-ZnO crystallites with similar crystallite size and specific surface area, the reaction rate constant of the C/ZnO at 800 °C ($k_m = 0.815 \text{ L} \cdot (\text{g} \cdot \text{min})^{-1}$) was much higher than that of the ZnO at 500 °C ($k_m = 0.209 \text{ L} \cdot (\text{g} \cdot \text{min})^{-1}$), indicating that carbon tiny particles attached on the surface of ZnO crystallites can greatly enhance the photocatalytic activity of ZnO. It was suspected that after UV light irradiation, the photo-induced electrons in the C/ZnO were transferred to and trapped into the attached carbon particles, resulting in the reduction of recombination rate of the photoinduced electron-hole pairs and the enhancement of photocatalytic activity of the specimen. The PL spectra of nanostructured semiconductor materials are relative to transfer behavior of the photoinduced electrons and holes, so that the intensities of the PL peaks reflect the separation and recombination of the photogenerated carriers [22,23]. Fig. 11 shows the PL spectra of the ZnO at 500 °C and the C/ZnO at 800 °C. It

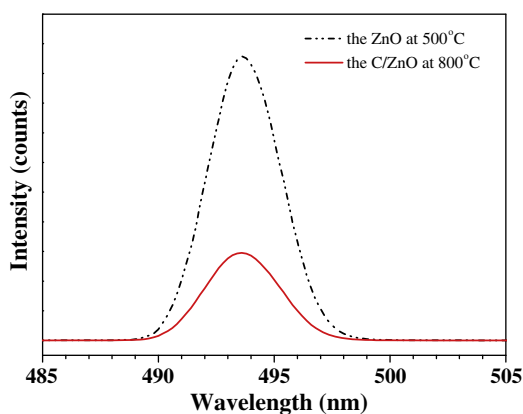


Fig. 11. PL emission spectra of the ZnO calcined at 500 °C and the C/ZnO calcined at 800 °C.

is clear that the intensity of the PL peak at 493.6 nm for the C/ZnO at 800 °C is smaller than that for the ZnO at 500 °C, which confirms that the carbon-coupling ZnO particles (i.e., the calcined C/ZnO) has lower recombination rate of the photoinduced electron–hole pairs and gives higher photocatalytic ability than the ZnO particles.

To examine if the carbon nanoparticles could be secured on the surface of ZnO particles in the C/ZnO, the C/ZnO powder calcined at 900 °C of 0.01 g was tested for its photocatalytic ability and the powder was recollected. The recycled powder was retested for its photocatalytic ability. Fig. 12 shows values of the corresponding k_m for each time test. It indicates that the photocatalytic ability of the recycled powder is similar to that of the fresh ones. The differences in the value of k_m between all these tests were less than 1%. This result implies that the carbon nanoparticles in the C/ZnO were firmly attached on the surfaces of ZnO particles.

4. Conclusions

A method combining precipitation and combustion techniques was used to prepare the C/ZnO photocatalysts. By adding glucose to the production procedure, the obtained C/ZnO precursor experienced a strong combustion at temperatures above 325 °C. The formed combustion gasses reduced the degree of particle agglomeration and the residual tiny carbon particles surrounded the zinc oxide crystallites, resulting in forming dispersive carbon-coupling ZnO particles with smaller particle sizes and higher specific surface area. The wurtzite–ZnO particles with high specific surface area and loose tiny carbons attachment to the ZnO crystallite surfaces exhibited high photocatalytic

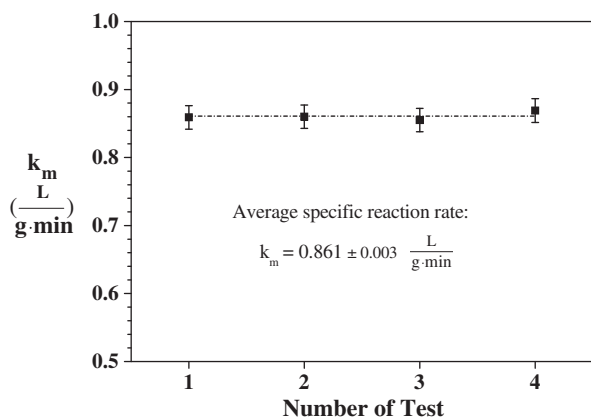


Fig. 12. The specific reaction rates (k_m) for the MB photocatalytic decomposition using the recycled C/ZnO calcined at 900 °C.

ability on UV light irradiation. The calcined C/ZnO particles possessed much higher photocatalytic abilities than the calcined ZnO particles and the P25. The C/ZnO particles calcined at 900 °C exhibited the best photocatalytic performance and had $k_m = 0.859 \text{ L} \cdot (\text{g} \cdot \text{min})^{-1}$ for photocatalytic decomposition of the MB in water under 365-nm UV light irradiation, which its photocatalytic abilities was much higher than those of the ZnO calcined at 700 °C ($k_m = 0.326 \text{ L} \cdot (\text{g} \cdot \text{min})^{-1}$) and the P25 ($k_m = 0.371 \text{ L} \cdot (\text{g} \cdot \text{min})^{-1}$).

References

- B. Dindar, S. Icli, Unusual photoreactivity of zinc oxide irradiated by concentrated sunlight, *Journal of Photochemistry and Photobiology A: Chemistry* 140 (2001) 263–268.
- D. Li, H. Haneda, Morphologies of zinc oxide particles and their effects on photocatalysis, *Chemosphere* 51 (2003) 129–137.
- T. Pauporte, J. Rathousky, Electrodeposited mesoporous ZnO thin films as efficient photocatalysts for the degradation of dye pollutants, *Journal of Physical Chemistry C* 111 (2007) 7639–7644.
- N. Sobana, M. Swaminathan, The effect of operational parameters on the photocatalytic degradation of acid red 18 by ZnO, *Separation and Purification Technology* 56 (2007) 101–107.
- X. Qiu, L. Li, J. Zheng, J. Liu, X. Sun, G. Li, Origin of the enhanced photocatalytic activities of semiconductors: a case study of ZnO doped with Mg^{2+} , *Journal of Physical Chemistry C* 112 (2008) 12242–12248.
- J.G. Yu, X.X. Yu, Hydrothermal synthesis and photocatalytic activity of zinc oxide hollow spheres, *Environmental Science & Technology* 42 (2008) 4902–4907.
- M. Castellano, E. Matijević, Uniform colloidal zinc compounds of various morphologies, *Chemistry of Materials* 1 (1989) 78–82.
- K. Fujita, K. Matsuda, S. Mitsuzawa, Formation of zinc oxide by homogeneous precipitation method, *Bulletin of the Chemical Society of Japan* 65 (1992) 2270–2271.
- S.C. Zhang, X.G. Li, Preparation of ZnO particles by precipitation transformation method and its inherent formation mechanisms, *Colloids and Surfaces A: Physicochemical and Engineering Aspects* 226 (2003) 35–44.
- Y. Wang, C. Zhang, S. Bi, G. Luo, Preparation of ZnO nanoparticles using the direct precipitation method in a membrane dispersion micro-structured reactor, *Powder Technology* 202 (2010) 130–136.
- C.-H. Lu, C.-H. Yeh, Influence of hydrothermal conditions on the morphology and particle size of zinc oxide powder, *Ceramics International* 26 (2000) 351–357.
- S. Musić, D. Dragević, S. Popović, M. Ivanda, Precipitation of ZnO particles and their properties, *Materials Letters* 59 (2005) 2388–2393.
- G. Colón, M.C. Hidalgo, J.A. Navío, E. Pulido Melián, O. González Díaz, J.M. Doña Rodríguez, Highly photoactive ZnO by amine capping-assisted hydrothermal treatment, *Applied Catalysis B: Environmental* 83 (2008) 30–38.
- C.-H. Lu, Y.-C. Lai, R.B. Kale, Influence of alkaline sources on the structural and morphological properties of hydrothermally derived zinc oxide powders, *Journal of Alloys and Compounds* 477 (2009) 523–528.
- Y. Lai, M. Meng, Y. Yu, X. Wang, T. Ding, Photoluminescence and photocatalysis of the flower-like nano-ZnO photocatalysts prepared by a facile hydrothermal method with or without ultrasonic assistance, *Applied Catalysis B: Environmental* 105 (2011) 335–345.
- A. El Hichou, M. Addou, J. Ebothé, M. Troyon, Influence of deposition temperature (T_s), air flow rate (f) and precursors on cathodoluminescence properties of ZnO thin films prepared by spray pyrolysis, *Journal of Luminescence* 113 (2005) 183–190.
- O. Milošević, D. Uskoković, L.J. Karanović, M. Tomasević-Canović, M. Trontelj, Synthesis of ZnO-based varistor precursor powders by means of the reaction spray process, *Journal of Materials Science* 28 (1993) 5211–5217.
- O. Milošević, B. Jordović, D. Uskoković, Preparation of fine spherical ZnO powders by an ultrasonic spray pyrolysis method, *Materials Letters* 19 (1994) 165–170.
- D. Li, H. Haneda, Synthesis of nitrogen-containing ZnO powders by spray pyrolysis and their visible-light photocatalysis in gas-phase acetaldehyde decomposition, *Journal of Photochemistry and Photobiology A: Chemistry* 155 (2003) 171–178.
- M.R. Hoffmann, S.T. Martin, W. Choi, D.W. Bahnemann, Environmental applications of semiconductor photocatalysis, *Chemical Reviews* 95 (1995) 69–96.
- L. Zheng, Y. Zheng, C. Chen, Y. Zhan, X. Lin, Q. Zheng, K. Wei, J. Zhu, Network structured SnO_2/ZnO heterojunction nanocatalyst with high photocatalytic activity, *Inorganic Chemistry* 48 (2009) 1819–1825.
- C. Ren, B. Yang, M. Wu, J. Xu, Z. Fu, Y. Iv, T. Guo, Y. Zhao, C. Zhu, Synthesis of Ag/ZnO nanorods array with enhanced photocatalytic performance, *Journal of Hazardous Materials* 182 (2010) 123–129.
- C. Tian, W. Li, K. Pan, Q. Zhang, G. Tian, W. Zhou, H. Fu, One pot synthesis of Ag nanoparticles modified ZnO microspheres in ethylene glycol medium and their enhanced photocatalytic performance, *Journal of Solid State Chemistry* 183 (2010) 2720–2725.
- Y. Zheng, L. Zheng, Y. Zhan, X. Lin, Q. Zheng, K. Wei, Ag/ZnO heterostructure nanocrystals: synthesis, characterization, and photocatalysis, *Inorganic Chemistry* 46 (2007) 6980–6986.
- W. Cun, Z. Jincai, W. Xinming, M. Bixian, S. Guoying, P. Ping'an, F. Jiamao, Preparation, characterization and photocatalytic activity of nano-sized ZnO/SnO_2 coupled photocatalysts, *Applied Catalysis B: Environmental* 39 (2002) 269–279.

- [26] L. Shi, C. Li, H. Gu, D. Fang, Morphology and properties of ultrafine SnO₂-TiO₂ coupled semiconductor particles, *Materials Chemistry and Physics* 62 (2000) 62–67.
- [27] C. Xu, L. Cao, G. Su, W. Liu, H. Liu, Y. Yu, X. Qu, Preparation of ZnO/Cu₂O compound photocatalyst and application in treating organic dyes, *Journal of Hazardous Materials* 176 (2010) 807–813.
- [28] N. Serpone, P. Maruthamuthu, P. Pichat, E. Pelizzetti, H. Hidaka, Exploiting the interparticle electron transfer process in the photocatalysed oxidation of phenol, 2-chlorophenol and pentachlorophenol: chemical evidence for electron and hole transfer between coupled semiconductors, *Journal of Photochemistry and Photobiology A: Chemistry* 85 (1995) 247–255.
- [29] H. Yu, Photocatalytic abilities of gel-derived P-doped TiO₂, *Journal of Physics and Chemistry of Solids* 68 (2007) 600–607.